HHS Public Access

Author manuscript

J Biomed Mater Res A. Author manuscript; available in PMC 2018 May 22.

Published in final edited form as:

J Biomed Mater Res A. 2017 May ; 105(5): 1281–1292. doi:10.1002/jbm.a.36013.

Effects of aging upon the host response to implants

Daniel Hachim[1,2], **Na Wang**[1], **Samuel T. Lopresti**[1,2], **Elizabeth C. Stahl**[1,3], **Yuta U. Umeda**[2], **Rahul D. Rege**[2], **Sean T. Carey**[4], **Deepa Mani**[1], and **Bryan N. Brown**[1,2,5]

[1]McGowan Institute for Regenerative Medicine, University of Pittsburgh, 450 Technology Drive, Pittsburgh, Pennsylvania 15219

[2]Department of Bioengineering, Swanson School of Engineering, University of Pittsburgh, 3700 O'Hara Street, Pittsburgh, Pennsylvania 15260

[3]Department of Pathology, University of Pittsburgh School of Medicine, University of Pittsburgh, 200 Lothrop St, Pittsburgh, Pennsylvania 15261

[4]Department of Chemical Engineering, Swanson School of Engineering, University of Pittsburgh, 3700 O'Hara Street, Pittsburgh, Pennsylvania 15260

[5]Department of Obstetrics, Gynecology and Reproductive Sciences, University of Pittsburgh School of Medicine, University of Pittsburgh, 300 Halket Street, Pittsburgh, Pennsylvania 15213

Abstract

Macrophage polarization during the host response is now a well-accepted predictor of outcomes following material implantation. Immunosenescence, dysregulation of macrophage function, and delayed resolution of immune responses in aged individuals have all been demonstrated, suggesting that host responses to materials in aged individuals should differ from those in younger individuals. However, few studies examining the effects of aging upon the host response have been performed. The present work sought to elucidate the impacts of aging upon the host response to polypropylene mesh implanted into 8-week-old and 18-month-old mice. The results showed that there are significant differences in macrophage surface marker expression, migration, and polarization during the early host macrophage response and delayed resolution of the host response in 18-month-old versus 8-week-old mice. These differences could not be attributed to cell-intrinsic defects alone, suggesting that the host macrophage response to implants is likely also dictated to a significant degree by the local tissue microenvironment. These results raise important questions about the design and testing of materials and devices often intended to treat aged individuals and suggest that an improved understanding of patient- and context-dependent macrophage responses has the potential to improve outcomes in aged individuals.

Keywords

macrophage; polarization; host response; aging; implant

Correspondence to: B. N. Brown; brownb@upmc.edu.

Additional Supporting Information may be found in the online version of this article.

INTRODUCTION

The host immune response to materials is an essential component of implant performance. Materials which evoke a strong chronic inflammatory response or foreign body reaction are logically subject to degradation and/or failure over time. This has led to a large and diverse set of approaches seeking to reduce or evade the host inflammatory response as a means of improving implant performance. These include tuning of surface topography,[1–5] porosity,[6–11] and chemistry[12–15] of the material, as well as the use of nonfouling surfaces and coatings[16–18] and decorating surfaces with matricellular proteins to prevent non-self-recognition.[19–21] These approaches have met with only modest improvements in the early response with few improvements in the long term. More recently, the concept of the host response as a predictor of implant performance has been revisited. [22,23] In particular, macrophages—considered the key drivers of the host immune response to implanted materials— have received considerable attention.[24–26] It is now well recognized that macrophages are not simply proinflammatory, cytotoxic mediators of inflammation. Rather, macrophages are now known to be capable of polarizing toward a multitude of phenotypic and functional profiles with roles in diverse processes including cancer, wound healing, development, and tissue regeneration among many others.[27–30] While it is a gross oversimplification of the *in vivo* reality, macrophages have been described as having M1 proinflammatory and M2 anti-inflammatory/regulatory phenotypes, representing extremes along a continuum of possible phenotypes.[31,32]

An increasing number of studies in the field of biomaterials and regenerative medicine have now begun to apply the macrophage M1/M2 paradigm, and have shown that macrophage phenotype can be modulated by biomaterials with improved tissue remodeling, integration, and long-term functional outcomes as a result.[10,23,33–37] For example, a recent study demonstrated that transient, early-stage (7 days postimplantation) shifts in macrophage polarization from an M1 to M2 phenotype at the host–implant interface mitigated the foreign body reaction to polypropylene mesh and improved implant integration downstream.[38] Studies such as this demonstrate the critical nature of the earliest events in the host–implant interaction in determining downstream integration and suggest that methods which seek to modulate, rather than avoid, this response will meet with greater success.

While temporal and spatial control of macrophage polarization toward an M1 or M2 phenotype can now be achieved in multiple ways,[39–41] the ability to effectively promote the desired phenotypic profile is likely predicated upon an in-depth, context- and tissue-dependent understanding of how host factors affect the response to biomaterials. A number of recent studies have highlighted the importance of the implantation site and/or the pathologic state of the tissue into which a biomaterial is implanted. For example, polyether–polyurethane sponge implants evoked distinct responses when placed in intraperitoneal versus subcutaneous locations[42] and polypropylene mesh implanted abdominally was shown to evoke a reduced inflammatory response compared to those implanted vaginally, [43] demonstrating differences in immune cell activity based upon implant location. Intraperitoneal implants in diabetic rats were associated with increases in inflammatory factors as compared to nondiabetic rats[44] and increased fibrosis was observed in lupus-prone mouse models,[45] demonstrating the effects of underlying pathology on the host response.

Another recent study showed differences in the host response to adhesive materials in animal models of colitis and colon cancer,[46] demonstrating that the observed host response was due to not only implant material composition but also the preimplantation state and cellular composition of the tissue of interest. Of note, the authors were able to use the information gleaned from these studies to create improved context- and disease-dependent materials for these applications. Thus, it has been suggested that the ideas of "biocompatibility," the host macrophage reaction, and ideal material requirements and modification strategies may need to be revisited on a disease, tissue, and even patient-by-patient basis.[47]

Aging is an unavoidable process known to affect multiple aspects of the immune system in both humans and animals.[48] While the effects of aging upon the adaptive immune system are increasingly well described, the phenotypic and functional changes within the innate immune system with aging are less clear. However, immunosenescence, dysregulation of macrophage function and polarization, and delayed resolution of acute immune responses in aged individuals have all been reported.[49–51] Therefore, it is logical that aging would also have effects on the host response to implantable materials. However, studies examining the effects of aging on the host response to implants and the implications of this response for long-term integration and function have not been performed. Thus, there is a clear need to elucidate the impacts of aging on the host response to develop implantable materials which more effectively address the needs of an increasingly aged population.

The purpose of this study was to evaluate the early host macrophage response and downstream integration following placement of polypropylene mesh in young (8-week-old) versus aged (18-month-old) mice.

MATERIALS AND METHODS

Materials

C57BL/6 female mice, 8–10-weeks-old and 18-months old, were obtained from the National Institute on Aging Mouse Colony. A polypropylene mesh, Gynemesh® PS (Ethicon, Somerville, NJ) was used. Bovine serum albumin (BSA) and histologic staining materials were purchased from Sigma Aldrich (St. Louis, MO). Rabbit anti-mouse arginase (Arg-1), inducible nitric oxide synthase (iNOS), CD68, and anti-rabbit, anti-rat, anti-goat Alexa-fluor (donkey) secondary antibodies were purchased from Abcam (Cambridge, MA). Rabbit anti-mouse iNOS, CD68, CD11b, and goat anti-mouse CD68 were purchased from Santa Cruz (Dallas, TX). Rabbit anti-mouse iNOS (ab3523) and Rabbit anti-mouse Arginase (ab91279) were purchased from Abcam (Cambridge, MA). Rat anti-mouse F4/80 was purchased from ABD Serotec (Raleigh, NC). Anti-rat Alexa-fluor 488 (donkey) and anti-rabbit Alexa-fluor 488 (donkey) were purchased from Thermo Fisher, Invitrogen (Pittsburgh, PA). DAPI was purchased from Thermo Fisher Scientific (Pittsburgh, PA). Qiagen RNEasy Mini Prep kits were purchased from Fisher Scientific (Pittsburgh, PA). High-capacity RNA-to-cDNA kits, Taqman gene expression assays, and Taqman Gene Expression Master Mix were purchased from Thermo Fisher, Invitrogen (Pittsburgh, PA). Vybrant Phagocytosis kit was purchased from Thermo Fisher, Invitrogen (Pittsburgh, PA). Sulfanilamide, phosphoric acid and N-1-napthylethylenediamine were purchased from Sigma-Aldrich (St. Louis, MO).

Mouse implantation model

An implantation model using C57BL/6 female mice, 8–10-weeks-old and 18-months-old, was used following proper housing and treatment procedures approved by the Institutional Animal Care and Use Committee (IACUC) of the University of Pittsburgh. NIH guidelines for the care and use of laboratory animals (NIH Publication #85–23 Rev. 1985) were observed. A power analysis was performed to determine that 7 animals per group was required to maintain a statistical power of at least 80%, based on previous studies using the same model.[38]

A midline incision was made and a subcutaneous pocket was created in the abdomen of each mouse to implant a 1-cm^2 piece of polypropylene mesh. 3–0 polycaprolactone sutures were used to close the incision, and then 0.5 mg/kg of Baytril and 0.2 mg/kg of Buprenex were administered for 3 days as antibiotic and analgesic, respectively. Buprenorphine (Buprenex), an opioid analgesic, has been studied and shown not to exert any effects or alterations in the immunological response, both acutely and chronically administered.[52,53] After 3, 7, 14, or 90 days, mice were euthanized and skin/mesh/muscle complex tissues were harvested and fixed for 72 h in neutral buffered formalin. Finally, fixed tissues were paraffin embedded and cross-sections of 7 μm were used for histological studies.

Histologic staining and evaluation

Paraffin-embedded tissue cross-sections were used for H&E, Alcian Blue, Masson's Trichrome, and Picro Sirius Red staining. H&E-, Alcian Blue-, and Masson's Trichrome-stained tissue sections were imaged on a Nikon Eclipse E600 microscope (Tokyo, Japan) at 10×, 20×, and 40×, respectively. Picro Sirius Red-stained tissue sections were imaged at 20× on a Nikon Eclipse TE2000-E (Tokyo, Japan), equipped with circularly polarized light.

ImageJ (version 1.48, NIH) equipped with a color deconvolution plug-in (version 1.5) was used to quantify glycosaminoglycans (GAGs) and collagen capsule surrounding mesh fibers at 3, 7, 14, and 90 days (3 different single fibers per sample, $N = 7$ each group) in images taken from histological tissue sections stained with Alcian Blue and Masson's Trichrome, respectively. In addition, the mean capsule thickness (including both the cellular reaction at the immediate implant surface and the surrounding collagen capsule) was calculated as the mean of apical, basal, and lateral measurements taken perpendicular to the surface of the mesh fiber in Masson's Trichrome-stained tissue sections.

A custom-designed algorithm (Mathworks MathLab, version R2015a, Natick, MA) was used to evaluate quantitatively the distribution of collagen fiber sizes surrounding mesh fibers at 90 days (3 different single fibers per sample, $N = 7$ each group) in images taken from histological tissue sections stained with Picro Sirius Red.

Immunolabeling and evaluation

Paraffin-embedded tissue sections were deparaffinized and hydrated in a series of xylene/alcohol/water. Incubation with proteinase K (1×) for 10 min at 37°C and/or boiling in citric acid buffer (pH = 6) for 20 min were performed to retrieve antigens. Slides were washed twice in TBST (25 mM Tris buffer + 0.1% tween 20). Then, a 5% donkey serum + 2% BSA

+ 0.1% Tween 20 + 0.1% Triton X-100 solution was used as blocking agent (2 h, RT). Table I lists the antibodies and concentrations used in this study.

All primary antibodies were incubated overnight at 4°C in blocking buffer. Secondary antibodies were incubated for 40 min at RT. Vectashield with DAPI mounting media (Vector laboratories, Burlingame, CA) was used to stain nuclei and mount. Images of centered single fibers were taken on a Nikon Eclipse E600 microscope equipped with epifluorescence at 40×. Cell counting using ImageJ (version 1.48, NIH) was performed to identify and quantify macrophage populations from cells surrounding single-centered mesh fibers (3 different single fibers, $N = 7$ for each group).

Harvest, culture, and polarization of bone marrow-derived macrophages

Bone marrow-derived macrophages were harvested from 8–10-week-old and 18-month-old C57BL/6 mice. Briefly, femur and tibiae were harvested and separated from muscle and connective tissue. Bones were cut at either end to expose bone marrow. Sterile syringe and needles were used to flush out bone marrow using macrophage differentiation media (DMEM, 10% FBS, 10% L-929 Supernatant, 1% Pen-Strep, 2% NEAA, 1% HEPES, 0.2% β-2 mercaptoethanol). Bone marrow lysate was reconstituted in media and filtered through a sterile cell filter. Cells were cultured for 7 days in media to differentiate them into macrophages. Following 7 days of differentiation culture, macrophages were treated polarizing regimens. Naïve macrophage (M0) controls were treated with basal media for 24 h. M1 (20 ng/mL IFN-γ and 100 ng/mL LPS) and M2 (20 ng/mL IL-4) polarizing cytokines were used to create proinflammatory and anti-inflammatory/regulatory macrophages, respectively.

Immunocytochemistry analysis

Cells were fixed with 2% paraformaldehyde (PFA) for 30 min and then washed in 1× PBS. Cells were blocked using 2% donkey serum, 1% BSA, 0.1% Triton X-100, and 0.1% Tween-20 for 1 h at room temperature. Primary antibodies were diluted in this blocking buffer as follows and incubated overnight at 4°C. Cells were washed in 1× PBS and incubated in fluorescent-labeled secondary antibodies for 1 h at room temperature. Cell nuclei were counterstained with DAPI. Table II lists the antibodies and concentrations used in this study. Images were taken in an array of 3 × 3 images per each well using a Carl Zeiss Observer.Z1 microscope and then the intensity of staining was analyzed using Cell Profiler Image Analysis Software (Broad Institute, Cambridge, MA) using the same number of cells for all tested conditions.

Gene expression analysis

Following treatments, macrophages were harvested for RNA using Qiagen RNEasy MiniPrep RNA Isolation Columns following standard protocol. RNA was quantified using a Nano-Drop Spectrophotometer. cDNA templates were created using Invitrogen High Capacity RNA-to-cDNA kits. Taqman Gene Expression assays were performed for the following markers: iNOS, IL-1β, IL-12β, TNF-α, IL-10, Arg, Fizz1, MRC1, PPARγ.

Nitric oxide assay

Following treatments, supernatant from macrophages were collected. Nitric oxide content was assayed using a Greiss Reagent system. Sulfanilamide (1% in 5% phosphoric acid) was added to supernatants for 10 min. Then, 0.1% *N*-1-napthylethylenediamine in water was added to the mixture for an additional 10 min. The absorbance at 540 nm was measured using a spectrophotometer.

Phagocytosis assay

Following treatments, cells were assayed for phagocytic ability using Vybrant Phagocytosis Assay kit. Cells were incubated in FITC-labeled dead *Escherichia coli* particles for 2 h in the cell culture incubator. Following thorough washing, the cells were fixed with 2% PFA for 30 min and washed with 1× PBS. Cell nuclei were counterstained with DAPI. Images were taken in an array of 3 × 3 images per each well using a Carl Zeiss Observer. Z1 microscope and then the FITC fluorescence intensity of staining was analyzed using Cell Profiler Image Analysis Software using the same number of cells for all tested conditions.

Statistical analysis

Comparisons of means were performed by either unpaired *t*-test (two-tailed), one-way or two-way analysis of variance (ANOVA), using at least $p < 0.05$ as statistical significance criteria followed by Tukey's test to compare groups and Sidak's test to compare time points. Shapiro-Wilk was used to test normality. All statistical tests were performed on GraphPad Prism V7 (La Jolla, California, USA).

RESULTS

Histomorphologic evaluation of the early host response

The overall histomorphologic appearance of the early host response to the implanted mesh materials in H&E-stained sections was largely similar in 8-week-old and 18-month-old mice (Fig. 1); however, the results suggested slower migration of mononuclear cells to the mesh surface in the 18-month-old group. Briefly, at 3 days, the site of remodeling was characterized by provisional matrix deposition and early invasion of the site by predominantly mononuclear cells with a small number of neutrophils remaining. Of note, though the number of cells within the site of remodeling was found to be quantitatively similar at the 3-day time point, there was an increased proportion of cells closer to the implant surface in the 8-week-old group as compared to the 18-month-old group. However, fewer cells were observed at the surface of the implant than those were observed in the area distant from the immediate surface in either group. By 7 days, additional neomatrix deposition with little to no organization was observed accompanied by angiogenesis in the peri-implant area. The response at 7 days was predominated by mononuclear cells in the area immediately surrounding the mesh, with spindle-shaped cells observed more distantly within the newly deposited matrix. The distribution of cells within the 20× images were similar for both 8-week-old and 18-month-old mice, though both a qualitative and quantitative decrease in cell density were noted for the 18-month-old group as compared to the 8-week-old group. The formation of multi-nucleated giant cells at the mesh surface was

observed in both groups at the 7-day time point and persisted throughout the remainder of the study. By 14 days, additional matrix deposition was observed, with a small degree of organization of the newly deposited matrix around the apical and basal aspects of the individual fibers. The number of vessels within the site of remodeling was observed to decrease, though the remaining vessels were more mature than was observed at 7 days. The response immediately surrounding the mesh was predominated by mononuclear cells with an increased proportion of spindle-shaped cells observed within remodeling site as compared to the 7-day time point. The qualitative and quantitative distribution of cells within the site of remodeling was similar for both groups at the 14-day time point.

Characterization of macrophage populations in the early host response

Macrophages and newly recruited monocytes were detected at the implanted mesh surface by immunostaining with commonly described surface markers: F4/80, CD68, and CD11b [Fig. 2(a)]. The number of $F4/80^+$ single-positive cells peaked at 7 days in both the 8- and 18-month-old mice, consistent with cell recruitment; however, there were significantly fewer $F4/80^+$ cells present in the 18-month-old mice at 3 days [Fig. 2(b)]. The number of $CD68^+$ cells remained consistent in the 8-week-old mice, but peaked at 7 days in the 18-month-old mice. In addition, there were significantly fewer $CD68^+$ cells present in the 18-month-old mice at 3 and 14 days. Very few cells expressed CD11b at the 3-day time point; however, the $CD11b^+$ cells peaked in both the 8- and 18-month-old mice at 7 days.

Few differences were observed between the two age groups in the double-labeled macrophages [Fig. 2(c)]. The number of $F4/80^+$ $CD68^+$ cells peaked at 7 days in both groups, and represented the greatest co-expression of macrophage markers at all time points, while very little co-expression was observed in the other groups. The number of $F4/80^+$ $CD11b^+$ cells increased at 7 days in 8-week-old mice, but was unchanged in the 18-month-old mice. The number of $CD68^+$ $CD11b^+$ macrophages was significantly decreased in 18-month-old mice compared to 8-week-old mice at 3 days. While the number of $CD68^+$ $CD11b^+$ macrophages did not change in 8-week-old mice, there was a decrease in the 18-month-old mice from 7 to 14 days. Additional representative images of the macrophage response across all time points and quantification by total cell percentage are included in Supporting Information, Figures S1–S4.

In vitro assessment of macrophage polarization and function

To determine whether there were inherent genetic or functional differences in the ability of macrophages to polarize in aged mice, bone marrow-derived macrophages were harvested from 8-week-old and 18-month-old C57BL/6 mice. Bone marrow-derived macrophages were treated using protocols for M1 (IFN-γ/LPS) and M2 (IL-4) as described above to determine their ability to polarize to these established phenotypes. Macrophage phenotype was assessed using indirect fluorescent antibody labeling for classical M1 (iNOS) and M2 (Arg-1) markers. Labeling showed that IFN-γ/LPS treatment resulted in significant increases in iNOS labeling in both 8-week-old and 18-month-old macrophages compared to both M0 (naïve, untreated) and M2 controls [Fig. 3(a)]. There was a significant increase in iNOS staining in macrophages harvested from 18-month-old as compared to 8-week-old mice in the IFN-γ/LPS treatment group. There were no differences in iNOS expression in

M0 baseline or M2-treated macrophages from 8-week-old and 18-month-old sources. IL-4 treatment resulted in a significant increase in Arg-1 labeling while IFN-γ/LPS treatment resulted in no significant difference [Fig. 3(b)]. There were no significant differences in Arg-1 labeling between 8-week-old and 18-month-old macrophages with any treatment regimen.

Macrophage functionality was assessed using phagocytosis assays and nitric oxide production as these are classical markers of macrophage activation. Phagocytosis was assessed using Vybrant FITC-labeled *E. coli* particles and subsequent mean fluorescent intensity determination as an approximation of the amount of particles phagocytosed [Fig. 3(c)]. Results showed that IFN-γ/LPS treatment in both 8-week-old and 18-month-old macrophages resulted in a significant increase in phagocytic particle uptake compared to M0 and M2 controls. There was no significant difference between 8-week-old and 18-month-old macrophage phagocytosis following any of the treatment regiments, suggesting that there are no intrinsic deficiencies in phagocytic functionality with aging. Nitric oxide production was assessed using the Greiss reagent system on supernatants following treatment [Fig. 3(d)]. Assays showed that 8-week-old and 18-month-old macrophages exhibited a significant increase in supernatant nitrite concentration with IFN-γ/LPS treatment compared to M0 and M2 treatment groups. There was also a significant increase in nitric oxide production from 8-week-old to 18-month-old macrophages in the IFN-γ/LPS treatment group. However, both the 8-week-old and 18-month-old macrophages retained the ability to produce nitric oxide in response to inflammatory signals.

Macrophage gene expression was determined using Taqman gene expression assays on common genes involved in the murine inflammatory process (iNOS, IL-1b, IL-12b, TNFa, IL-10, Arg-1, Fizz1, Mrc1, and PPARγ). Gene expression analysis showed that treatment of 8-week-old and 18-month-old bone marrow-derived macrophages with IFN-γ/LPS or IL-4 resulted in gene expression patterns which are indicative of M1 and M2 polarization, respectively [Fig. 3(e)]. No differences in gene expression were observed between macrophages harvested from 8-week-old and 18-month-old mice following either IFN-γ/LPS or IL-4 treatment. These findings illustrate that the ability of both 8-week-old and 18-month-old macrophages to polarize toward M1 and M2 phenotypes remain intact, complementing previously published literature in the field.[51]

In vivo macrophage polarization profile in the early host response

Macrophage polarization to an M1 or M2 state was evaluated *in vivo* using inducible nitric oxide synthase (iNOS) or arginase-1 (Arg-1) expression, respectively [Fig. 4(a)]. Arg-1 expression was induced significantly at 7 days in the 8-week-old mice, but remained unchanged in 18-month-old mice, suggesting a deficit in M2 polarization in aged mice **[**Fig. 4(b)**].** At 14 days postimplantation, Arg-1 expression in the 8-week-old group returned to basal levels similar to the 18-month-old mice. Interestingly, co-labeling Arg-1 with CD68 revealed that $CD68^+$ cells accounted for the vast majority of Arg-1 expressing cells at all time points. On the other hand, iNOS expression was induced significantly at 7 days in the 18-month-old mice, but remained unchanged in the 8-week-old mice [Fig. 4(c, d)], demonstrating an M1 profile in the aged cells. While both 8-week-old and 18-month-old

mice showed reduced iNOS expression at 14 days, the 18-month-old cells retained a higher iNOS expression compared to 8-week-old mice. Co-labeling of iNOS with CD68 accounted for very few of the $iNOS^+$ cells, suggesting that another cell type is responsible for iNOS expression. The total cell percentage of M1/M2 macrophage polarization is included in Supporting Information, Figure S6.

In vivo effects of the aged microenvironment upon the host response

As the above results suggest that local tissue cues could have effects on the profile and functionality of macrophages in the host response, the GAG composition of the local microenvironment was evaluated by means of an Alcian Blue histological staining. GAG composition was evaluated in this study as GAGs represent an important structural component of the tissue extracellular matrix, with key roles in regulating macrophage polarization both acting as a substrate for early infiltrating macrophage populations and by sequestering signaling molecules.[54,55] The presence of GAGs (blue) was detected in both implanted mice groups [Fig. 5(a, b)], with no differences observed at 3, 14, and 90 days. Interestingly, at 7 days, the 18-month-old group had significantly less GAG deposition, corresponding temporally with the observed changes in macrophage recruitment and polarization.

Long-term *in vivo* evaluation of fibrotic capsule deposition

Fibrotic capsule deposition and composition were used as metrics to determine the impact of aging on the host response against polypropylene mesh in the long term (90 days). The capsule was defined as the distance between the implant surface and the outer aspect of the dense collagenous matrix surrounding the mesh fibers [Fig. 6(a), black arrow], inclusive of the cell layer adjacent to the surface and within the capsule [Fig. 6(a), green arrow]. Quantitative analysis revealed no difference in the area or thickness of the collagenous portion between the 8-week-old and 18-month-old implanted mice [Fig. 6(b, c)]. Further assessment of the composition of the fibrotic capsule revealed no differences in the capsule composition between the two age groups [Fig. 6(e, f)]. However, 18-month-old mice were observed to have a significant increase in both the thickness of the cell layer and total number of cells at the mesh fiber surface at 90 days [Fig. 6(c, d)], suggesting an unresolved host response to the implanted mesh.

DISCUSSION

By 2050, the number of individuals over the age of 65 is expected to increase by 71% to nearly 2 billion worldwide, with the number of US citizens over the age of 65 surpassing 20% by 2030.[56] As a result, there is an increasing demand for implantable medical devices intended to treat age-related disorders. Despite the increasing usage of implantable medical devices in aged patient populations, the impacts of aging on the host response have never been deeply investigated. The literature which does exist on the topic largely hypothesizes the potential impacts of aging on the host response[57] based on the known effects of aging on the immune system and on wound healing, though a small number of relevant studies have recently been performed. [58–61] In one study, Sicari et al. demonstrated that increased source animal age of tissue-derived biomaterials, such as decellularized ECM constructs, reduced

the number of M2 polarized macrophages and lead to a poor outcome of tissue remodeling compared to young host-derived biomaterials. [58] Olivares-Navarrette et al. showed that titanium implants with varying roughness and surface energy yielded lower bone-to-implant contact, neovascularization, and bone formation in aged rats.[59] Finally, *in vitro* analyses of senescent macrophages induced by extended culture demonstrated deficits in phagocytosis and cytokine release in response to titanium dioxide particles and polystyrene materials, suggesting macrophage function may be compromised in the aged host response.[60,61]

The findings of this study suggest that the host macrophage response to polypropylene mesh implants is delayed, dysregulated, and unresolved in aged animals as compared to young. Specifically, it was observed that there was a deficit in early responding macrophage populations in 18-month-old mice as compared to 8-week-old mice at 3 days and retarded recruitment of additional macrophage populations at 7 days. The population which was present at the 7-day time point was found to express significantly less Arg-1 and significantly more iNOS in 18-month-old mice as compared to 8-week-old, suggesting a more M1-like proinflammatory profile. Previous studies have shown the 7–14-day postimplantation time frame to be significantly predictive of downstream outcomes, with higher numbers of M2 polarized cells and higher ratios of M2:M1 cells as indicators of improved integration and remodeling.[23,36–38] Thus, this finding indicates the potential for poor downstream integration and remodeling in 18-month-old mice.

While the composition and thickness of the collagenous portion of the capsule was found to be similar between 8-week-old and 18-month-old mice, this study also demonstrated higher cellularity within the tissue capsule surrounding the implants at 90 days postimplantation, suggesting an unresolved or ongoing inflammatory response. The findings of delayed, dysregulated, and unresolved host responses in this study correlate well with observations of dysregulated inflammation and delayed resolution of inflammatory responses to pathogen and in wound healing.[48] For example, a study of punch biopsies from healthy human subjects between the ages of 19 and 96 years old postwounding showed that the macrophage response in aged subjects peaked at 84 days as opposed to 7 days in younger subjects.[62] The delayed infiltration of macrophages in wound healing has been associated with poor re-epithelialization, reduced angiogenesis, deficits in collagen deposition, and decreased wound strength.[63] Altered immune responses to wounding or pathogens in aged individuals have largely been attributed to altered function of the adaptive immune system; however, multiple studies have noted the impacts of aging upon the innate immune compartment. [49–51] The studies which have observed immune dysfunction in aged macrophage populations have largely been performed using tissue-derived macrophages while the function of macrophages derived from the bone marrow has been shown to remain largely intact in multiple studies,[50,51] suggesting that age-related changes in the local tissue microenvironment may play a role in the observed dysfunction.[64,65]

In this study, bone marrow-derived macrophages harvested from 8-week-old and 18-month-old mice were subjected to standard M1 and M2 polarization regimes. The results demonstrate that both 8-week-old and 18-month-old macrophages retained the ability to polarize toward M1 and M2 phenotypes, and were functionally intact. Few differences between polarized macrophages harvested from the bone marrow of 8-week-old and 18-

month-old mice were noted; however, the expression of iNOS and production of NO were found to be higher in 18-month-old mice as compared to 8-week-old mice. These results correlate well with the finding of larger numbers of recruited $iNOS^+$ cells present within the remodeling site of implants in 18-month-old animals. This cell population was found to be largely separate from the Arg-1 expressing $CD68^+$ population in both 8-week-old and 18-month-old mice, suggesting the possibility of multiple, distinct macrophage populations participating in the host response.

Indeed, distinct macrophage populations identified as tissue-resident versus circulating with unique phenotypes and functions are widely identified in the literature. Each of these populations likely plays a distinct role in tissue homeostasis and the response to injury and pathogen on a tissue-by-tissue basis. In the liver, several studies have identified differential roles for $CD68^+$ tissue-resident Kupffer cells and $CD11b^+$ infiltrating bone marrow-derived macrophages in pathogen clearance and tumor cell destruction, respectively. [66–68] A number of recent studies have now described shifts in the proportions of tissue-resident versus circulating cells occurring within individual tissues with age and with important implications for the host response and outcomes following injury. For example, aging of cardiac muscle leads to progressive replacement of embryonic macrophages with bone marrow-derived macrophages.[67] The infiltrating macrophages were found to have a profibrotic gene signature, leading to impaired tissue regeneration that could be reversed by inhibiting monocyte recruitment.[69–71]

In this study, $CD68^+$ cells remained unchanged temporally in the 8-week-old mice, suggesting the possibility of a local cell origin as opposed to recruitment from bone marrow. Furthermore, this $CD68^+$ population co-localized with arginase-1 and was significantly decreased at the earliest time point in the 18-month-old animals. While the exact origin of these cells remains unclear, the recruitment and polarization of this population likely represents a key event which drives the downstream host response. A recent study showed that a reservoir of peritoneal cavity macrophages exists which can rapidly infiltrate injured organs in response to cell death signals.[54] This infiltration was found to occur rapidly (2–3 days postinjury) across the mesothelial lining of the peritoneum and into deeper tissue locations. Of significant interest, this population also assumed an alternatively activated M2-like phenotype upon arrival at the injury site. While the full set of mechanisms by which these cells are able to rapidly infiltrate tissues outside of the peritoneal cavity is unknown, the study demonstrated that the migration was dependent on CD44, the receptor for hyaluronan. While the role of changes in the local tissue microenvironment was not investigated deeply in this study, a reduction in the presence or production of glycosaminoglycan constituents, including hyaluronan, at early time points in the host response could have led to a reduction in the recruitment of early responding cells and/or changes in their polarization profile.

Taken together, the results of this work suggest that there are significant differences between the host response to materials in young and aged animals. These differences could not be accounted for by age-related accumulation of cell-intrinsic defects alone, and it is likely that the local tissue microenvironment also plays a large role in dictating the host response regardless of material composition. This study used only a limited set of surface markers and

makes inferences about the origin of cells based on these markers. Further study is necessary to determine the specific origin of the cells which participate in the host response in young and old animals as well as to clearly determine their *in vivo* phenotype and functional profile. However, it is clear that there are differences in the host response between young and aged animals, and that a better understanding of these differences will help to design materials and strategies that more effectively modulate the host immune response in aged individuals.

Supplementary Material

Refer to Web version on PubMed Central for supplementary material.

Acknowledgments

Contract grant sponsor: National Institutes of Health; contract grant numbers: K12HD043441, R03AG043606, R21GM107882, and T32EB001026

The content is solely the responsibility of the authors and does not necessarily represent the official views of the National Institutes of Health. The funding source had no involvement in the study design, collection of data, analysis of data, interpretation of data, writing of the report, or the decision to submit for publication. The authors would like to thank Kelley Brown for her support with histologic staining. The authors report no conflict of interest.

References

1. Rice JM, Hunt JA, Gallagher JA, Hanarp P, Sutherland DS, Gold J. Quantitative assessment of the response of primary derived human osteoblasts and macrophages to a range of nanotopography surfaces in a single culture model in vitro. Biomaterials. 2003; 24:4799–4818. [PubMed: 14530077]
2. Paul NE, Skazik C, Harwardt M, Bartneck M, Denecke B, Klee D, Salber J, Zwadlo-Klarwasser G. Topographical control of human macrophages by a regularly microstructured polyvinylidene fluoride surface. Biomaterials. 2008; 29:4056–4064. [PubMed: 18667233]
3. Bota PC, Collie AM, Puolakkainen P, Vernon RB, Sage EH, Ratner BD, Stayton PS. Biomaterial topography alters healing in vivo and monocyte/macrophage activation in vitro. J Biomed Mater Res A. 2010; 95:649–657. [PubMed: 20725970]
4. Collie AM, Bota PC, Johns RE, Maier RV, Stayton PS. Differential monocyte/macrophage interleukin-1beta production due to biomaterial topography requires the beta2 integrin signaling pathway. J Biomed Mater Res A. 2011; 96:162–169. [PubMed: 21105164]
5. Hotchkiss KM, Reddy GB, Hyzy SL, Schwartz Z, Boyan BD, Olivares-Navarrete R. Titanium surface characteristics, including topography and wettability, alter macrophage activation. Acta Biomater. 2016; 31:425–434. [PubMed: 26675126]
6. Brauker JH, Carr-Brendel VE, Martinson LA, Crudele J, Johnston WD, Johnson RC. Neovascularization of synthetic membranes directed by membrane microarchitecture. J Biomed Mater Res. 1995; 29:1517–1524. [PubMed: 8600142]
7. Fleckman P, Usui M, Zhao G, Underwood R, Maginness M, Marshall A, Glaister C, Ratner B, Olerud J. Cutaneous and inflammatory response to long-term percutaneous implants of sphere-templated porous/solid poly(HEMA) and silicone in mice. J Biomed Mater Res A. 2012; 100:1256–1268. [PubMed: 22359383]
8. Fukano Y, Usui ML, Underwood RA, Isenhath S, Marshall AJ, Hauch KD, Ratner BD, Olerud JE, Fleckman P. Epidermal and dermal integration into sphere-templated porous poly(2-hydroxyethyl methacrylate) implants in mice. J Biomed Mater Res A. 2010; 94:1172–1186. [PubMed: 20694984]
9. Karp RD, Johnson KH, Buoen LC, Ghobrial HK, Brand I, Brand KG. Tumorigenesis by Millipore filters in mice: Histology and ultrastructure of tissue reactions as related to pore size. J Natl Cancer Inst. 1973; 51:1275–1285. [PubMed: 4583375]

10. Sussman EM, Halpin MC, Muster J, Moon RT, Ratner BD. Porous implants modulate healing and induce shifts in local macrophage polarization in the foreign body reaction. Ann Biomed Eng. 2014; 42:1508–1516. [PubMed: 24248559]
11. Underwood RA, Usui ML, Zhao G, Hauch KD, Takeno MM, Ratner BD, Marshall AJ, Shi X, Olerud JE, Fleckman P. Quantifying the effect of pore size and surface treatment on epidermal incorporation into percutaneously implanted sphere-templated porous biomaterials in mice. J Biomed Mater Res A. 2011; 98:499–508. [PubMed: 21681942]
12. Blaszykowski C, Sheikh S, Thompson M. Surface chemistry to minimize fouling from blood-based fluids. Chem Soc Rev. 2012; 41:5599–5612. [PubMed: 22772072]
13. Brodbeck WG, Shive MS, Colton E, Nakayama Y, Matsuda T, Anderson JM. Influence of biomaterial surface chemistry on the apoptosis of adherent cells. J Biomed Mater Res. 2001; 55:661–668. [PubMed: 11288096]
14. MacEwan, MR., Brodbeck, WG., Matsuda, T., Anderson, JM. Monocyte/lymphocyte interactions and the foreign body response: In vitro effects of biomaterial surface chemistry. J Biomed Mater Res A; Student Research Award in the Undergraduate Degree Candidate category, 30th Annual Meeting of the Society for Biomaterials; Memphis, Tennessee. April 27–30, 2005; 2005. p. 285-293.
15. Wilson CJ, Clegg RE, Leavesley DI, Pearcy MJ. Mediation of biomaterial–cell interactions by adsorbed proteins: A review. Tissue Eng. 2005; 11:1–18. [PubMed: 15738657]
16. Kingshott PGHJ. Surfaces that resist bioadhesion. Curr Opin Solid State Mater Sci. 1999; 4:403–412.
17. Zhang L, Cao Z, Bai T, Carr L, Ella-Menye JR, Irvin C, Ratner BD, Jiang S. Zwitterionic hydrogels implanted in mice resist the foreign-body reaction. Nat Biotechnol. 2013; 31:553–556. [PubMed: 23666011]
18. Zhang Z, Zhang M, Chen S, Horbett TA, Ratner BD, Jiang S. Blood compatibility of surfaces with superlow protein adsorption. Biomaterials. 2008; 29:4285–4291. [PubMed: 18722010]
19. Finley MJ, Clark KA, Alferiev IS, Levy RJ, Stachelek SJ. Intracellular signaling mechanisms associated with CD47 modified surfaces. Biomaterials. 2013; 34:8640–8649. [PubMed: 23948164]
20. Finley MJ, Rauova L, Alferiev IS, Weisel JW, Levy RJ, Stachelek SJ. Diminished adhesion and activation of platelets and neutrophils with CD47 functionalized blood contacting surfaces. Biomaterials. 2012; 33:5803–5811. [PubMed: 22613135]
21. Tengood JE, Levy RJ, Stachelek SJ. The use of CD47-modified biomaterials to mitigate the immune response. Exp Biol Med (Maywood). 2016; 241:1033–1041. [PubMed: 27190273]
22. Bryers JD, Giachelli CM, Ratner BD. Engineering biomaterials to integrate and heal: The biocompatibility paradigm shifts. Biotechnol Bioeng. 2012; 109:1898–1911. [PubMed: 22592568]
23. Brown BN, Londono R, Tottey S, Zhang L, Kukla KA, Wolf MT, Daly KA, Reing JE, Badylak SF. Macrophage phenotype as a predictor of constructive remodeling following the implantation of biologically derived surgical mesh materials. Acta Biomater. 2012; 8:978–987. [PubMed: 22166681]
24. Brown BN, Ratner BD, Goodman SB, Amar S, Badylak SF. Macrophage polarization: An opportunity for improved outcomes in biomaterials and regenerative medicine. Biomaterials. 2012; 33:3792–3802. [PubMed: 22386919]
25. Brown BN, Sicari BM, Badylak SF. Rethinking regenerative medicine: A macrophage-centered approach. Front Immunol. 2014; 5:510. [PubMed: 25408693]
26. Miron RJ, Bosshardt DD. OsteoMacs: Key players around bone biomaterials. Biomaterials. 2016; 82:1–19. [PubMed: 26735169]
27. Gordon S, Taylor PR. Monocyte and macrophage heterogeneity. Nat Rev Immunol. 2005; 5:953–964. [PubMed: 16322748]
28. Mantovani A, Sica A, Sozzani S, Allavena P, Vecchi A, Locati M. The chemokine system in diverse forms of macrophage activation and polarization. Trends Immunol. 2004; 25:677–686. [PubMed: 15530839]
29. Mills CD. M1 and M2 macrophages: Oracles of health and disease. Crit Rev Immunol. 2012; 32:463–488. [PubMed: 23428224]

30. Wynn TA, Chawla A, Pollard JW. Macrophage biology in development, homeostasis and disease. Nature. 2013; 496:445–455. [PubMed: 23619691]
31. Mosser DM, Edwards JP. Exploring the full spectrum of macrophage activation. Nat Rev Immunol. 2008; 8:958–969. [PubMed: 19029990]
32. Xue J, Schmidt SV, Sander J, Draffehn A, Krebs W, Quester I, De Nardo D, Gohel TD, Emde M, Schmidleithner L, et al. Transcriptome-based network analysis reveals a spectrum model of human macrophage activation. Immunity. 2014; 40:274–288. [PubMed: 24530056]
33. Guo R, Merkel AR, Sterling JA, Davidson JM, Guelcher SA. Substrate modulus of 3D-printed scaffolds regulates the regenerative response in subcutaneous implants through the macrophage phenotype and Wnt signaling. Biomaterials. 2015; 73:85–95. [PubMed: 26406449]
34. Keeney M, Waters H, Barcay K, Jiang X, Yao Z, Pajarinen J, Egashira K, Goodman SB, Yang F. Mutant MCP-1 protein delivery from layer-by-layer coatings on orthopedic implants to modulate inflammatory response. Biomaterials. 2013; 34:10287–10295. [PubMed: 24075408]
35. Mokarram N, Merchant A, Mukhatyar V, Patel G, Bellamkonda RV. Effect of modulating macrophage phenotype on peripheral nerve repair. Biomaterials. 2012; 33:8793–8801. [PubMed: 22979988]
36. Spiller KL, Nassiri S, Witherel CE, Anfang RR, Ng J, Nakazawa KR, Yu T, Vunjak-Novakovic G. Sequential delivery of immunomodulatory cytokines to facilitate the M1-to-M2 transition of macrophages and enhance vascularization of bone scaffolds. Biomaterials. 2015; 37:194–207. [PubMed: 25453950]
37. Brown BN, Valentin JE, Stewart-Akers AM, McCabe GP, Badylak SF. Macrophage phenotype and remodeling outcomes in response to biologic scaffolds with and without a cellular component. Biomaterials. 2009; 30:1482–1491. [PubMed: 19121538]
38. Hachim D, LoPresti ST, Yates CC, Brown BN. Shifts in macrophage phenotype at the biomaterial interface via IL-4 eluting coatings are associated with improved implant integration. Biomaterials. 2016; 112:95–107. [PubMed: 27760399]
39. Alvarez MM, Liu JC, Trujillo-de Santiago G, Cha BH, Vishwakarma A, Ghaemmaghami AM, Khademhosseini A. Delivery strategies to control inflammatory response: Modulating M1-M2 polarization in tissue engineering applications. J Control Release. 2016
40. Garash R, Bajpai A, Marcinkiewicz BM, Spiller KL. Drug delivery strategies to control macrophages for tissue repair and regeneration. Exp Biol Med (Maywood). 2016; 241:1054–1063. [PubMed: 27190256]
41. Vishwakarma A, Bhise NS, Evangelista MB, Rouwkema J, Dokmeci MR, Ghaemmaghami AM, Vrana NE, Khademhosseini A. Engineering immunomodulatory biomaterials to tune the inflammatory response. Trends Biotechnol. 2016; 34:470–482. [PubMed: 27138899]
42. Mendes JB, Campos PP, Ferreira MA, Bakhle YS, Andrade SP. Host response to sponge implants differs between subcutaneous and intraperitoneal sites in mice. J Biomed Mater Res B Appl Biomater. 2007; 83:408–415. [PubMed: 17415768]
43. Pierce LM, Rao A, Baumann SS, Glassberg JE, Kuehl TJ, Muir TW. Long-term histologic response to synthetic and biologic graft materials implanted in the vagina and abdomen of a rabbit model. Am J Obstet Gynecol. 2009; 200:546 e1–548. [PubMed: 19286140]
44. Oviedo-Socarras T, Vasconcelos AC, Barbosa IX, Pereira NB, Campos PP, Andrade SP. Diabetes alters inflammation, angiogenesis, and fibrogenesis in intraperitoneal implants in rats. Microvasc Res. 2014; 93:23–29. [PubMed: 24594441]
45. Campos PP, Vasconcelos AC, Ferreira MA, Andrade SP. Alterations in the dynamics of inflammation, proliferation and apoptosis in subcutaneous implants of lupus-prone mice. Histol Histopathol. 2011; 26:433–442. [PubMed: 21360436]
46. Oliva N, Carcole M, Beckerman M, Seliktar S, Hayward A, Stanley J, Parry NM, Edelman ER, Artzi N. Regulation of dendrimer/dextran material performance by altered tissue microenvironment in inflammation and neoplasia. Sci Transl Med. 2015; 7:272ra11.
47. Ratner BD. Healing with medical implants: The body battles back. Sci Transl Med. 2015; 7:272fs4.
48. Stahl EC, Brown BN. Cell therapy strategies to combat immunosenescence. Organogenesis. 2015; 11:159–172. [PubMed: 26588595]

49. Sebastián, C., Lloberas, J., Celada, A. Molecular and cellular aspects of macrophage aging. In: Fulop, T.Franceschi, C.Hirokawa, K., Pawelec, G., editors. Handbook on Immunosenescence. Netherlands: Springer; 2009. p. 919-945.
50. Linehan E, Dombrowski Y, Snoddy R, Fallon PG, Kissenpfennig A, Fitzgerald DC. Aging impairs peritoneal but not bone marrow-derived macrophage phagocytosis. Aging Cell. 2014; 13:699–708. [PubMed: 24813244]
51. Mahbub S, Deburghgraeve CR, Kovacs EJ. Advanced age impairs macrophage polarization. J Interferon Cytokine Res. 2012; 32:18–26. [PubMed: 22175541]
52. Sacerdote P. Opioids and the immune system. Palliat Med. 2006; 20:s9–15. [PubMed: 16764216]
53. Martucci C, Panerai AE, Sacerdote P. Chronic fentanyl or buprenorphine infusion in the mouse: Similar analgesic profile but different effects on immune responses. Pain. 2004; 110:385–392. [PubMed: 15275790]
54. Wang J, Kubes P. A reservoir of mature cavity macrophages that can rapidly invade visceral organs to affect tissue repair. Cell. 2016; 165:668–678. [PubMed: 27062926]
55. den Dekker E, Grefte S, Huijs T, ten Dam GB, Versteeg EM, van den Berk LC, Bladergroen BA, van Kuppevelt TH, Figdor CG, Torensma R. Monocyte cell surface glycosaminoglycans positively modulate IL-4-induced differentiation toward dendritic cells. J Immunol. 2008; 180:3680–3688. [PubMed: 18322173]
56. Ortman, JM., Howard Hogan, VAV. An aging nation: The older population in the United States. US Census Bureau; 2014.
57. Rao, ANAMN., Grainger, DW. Aging and the host response to implanted biomaterials. In: Badylak, SF., editor. Host Response to Biomaterials: The Impact of Host Response on Biomaterial Selection. London: Elsevier; 2015.
58. Sicari BM, Johnson SA, Siu BF, Crapo PM, Daly KA, Jiang H, Medberry CJ, Tottey S, Turner NJ, Badylak SF. The effect of source animal age upon the in vivo remodeling characteristics of an extracellular matrix scaffold. Biomaterials. 2012; 33:5524–5533. [PubMed: 22575834]
59. Olivares-Navarrete R, Raines AL, Hyzy SL, Park JH, Hutton DL, Cochran DL, Boyan BD, Schwartz Z. Osteoblast maturation and new bone formation in response to titanium implant surface features are reduced with age. J Bone Miner Res. 2012; 27:1773–1783. [PubMed: 22492532]
60. Holt DJ, Grainger DW. Senescence and quiescence induced compromised function in cultured macrophages. Biomaterials. 2012; 33:7497–7507. [PubMed: 22809642]
61. Bruno ME, Sittner M, Cabrini RL, Guglielmotti MB, Olmedo DG, Tasat DR. In vitro age dependent response of macrophages to micro and nano titanium dioxide particles. J Biomed Mater Res A. 2015; 103:471–478. [PubMed: 24733814]
62. Ashcroft GS, Horan MA, Ferguson MW. Aging alters the inflammatory and endothelial cell adhesion molecule profiles during human cutaneous wound healing. Lab Invest. 1998; 78:47–58. [PubMed: 9461121]
63. Ashcroft GS, Mills SJ, Ashworth JJ. Ageing and wound healing. Biogerontology. 2002; 3:337–345. [PubMed: 12510172]
64. Stout RD, Suttles J. Immunosenescence and macrophage functional plasticity: Dysregulation of macrophage function by age-associated microenvironmental changes. Immunol Rev. 2005; 205:60–71. [PubMed: 15882345]
65. Gomez CR, Nomellini V, Faunce DE, Kovacs EJ. Innate immunity and aging. Exp Gerontol. 2008; 43:718–728. [PubMed: 18586079]
66. Kinoshita M, Uchida T, Sato A, Nakashima M, Nakashima H, Shono S, Habu Y, Miyazaki H, Hiroi S, Seki S. Characterization of two F4/80-positive Kupffer cell subsets by their function and phenotype in mice. J Hepatol. 2010; 53:903–910. [PubMed: 20739085]
67. Molawi K, Wolf Y, Kandalla PK, Favret J, Hagemeyer N, Frenzel K, Pinto AR, Klapproth K, Henri S, Malissen B, et al. Progressive replacement of embryo-derived cardiac macrophages with age. J Exp Med. 2014; 211:2151–2158. [PubMed: 25245760]
68. Ikarashi M, Nakashima H, Kinoshita M, Sato A, Nakashima M, Miyazaki H, Nishiyama K, Yamamoto J, Seki S. Distinct development and functions of resident and recruited liver Kupffer cells/macrophages. J Leukoc Biol. 2013; 94:1325–1336. [PubMed: 23964119]

69. Pinto AR, Godwin JW, Chandran A, Hersey L, Ilinykh A, Debuque R, Wang L, Rosenthal NA. Age-related changes in tissue macrophages precede cardiac functional impairment. Aging (Albany NY). 2014; 6:399–413. [PubMed: 24861132]

70. Epelman S, Lavine KJ, Beaudin AE, Sojka DK, Carrero JA, Calderon B, Brija T, Gautier EL, Ivanov S, Satpathy AT, et al. Embryonic and adult-derived resident cardiac macrophages are maintained through distinct mechanisms at steady state and during inflammation. Immunity. 2014; 40:91–104. [PubMed: 24439267]

71. Lavine KJ, Epelman S, Uchida K, Weber KJ, Nichols CG, Schilling JD, Ornitz DM, Randolph GJ, Mann DL. Distinct macrophage lineages contribute to disparate patterns of cardiac recovery and remodeling in the neonatal and adult heart. Proc Natl Acad Sci USA. 2014; 111:16029–16034. [PubMed: 25349429]

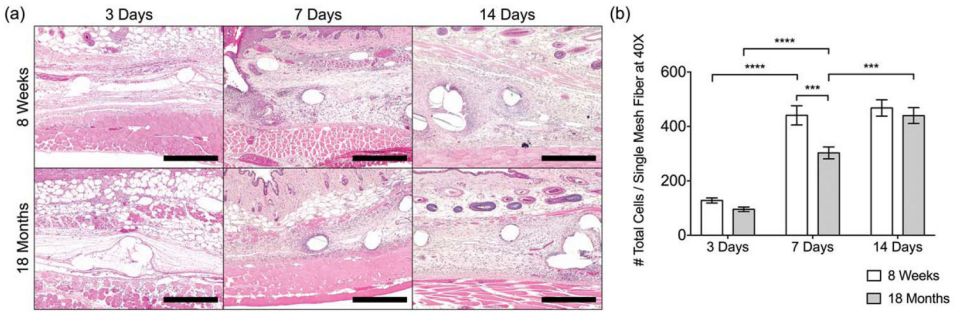

FIGURE 1.

(a) Images of H&E-stained tissue cross-sections at 10× and (b) total cell counts (DAPI) surrounding single mesh fibers in 40× images at 3, 7, and 14 days. Scale bars represent 200 μm. Bars represent the mean ± SEM. Statistical significance as (***) $p < 0.001$ and (****) $p < 0.0001$. All other differences are nonsignificant. $N = 7$.

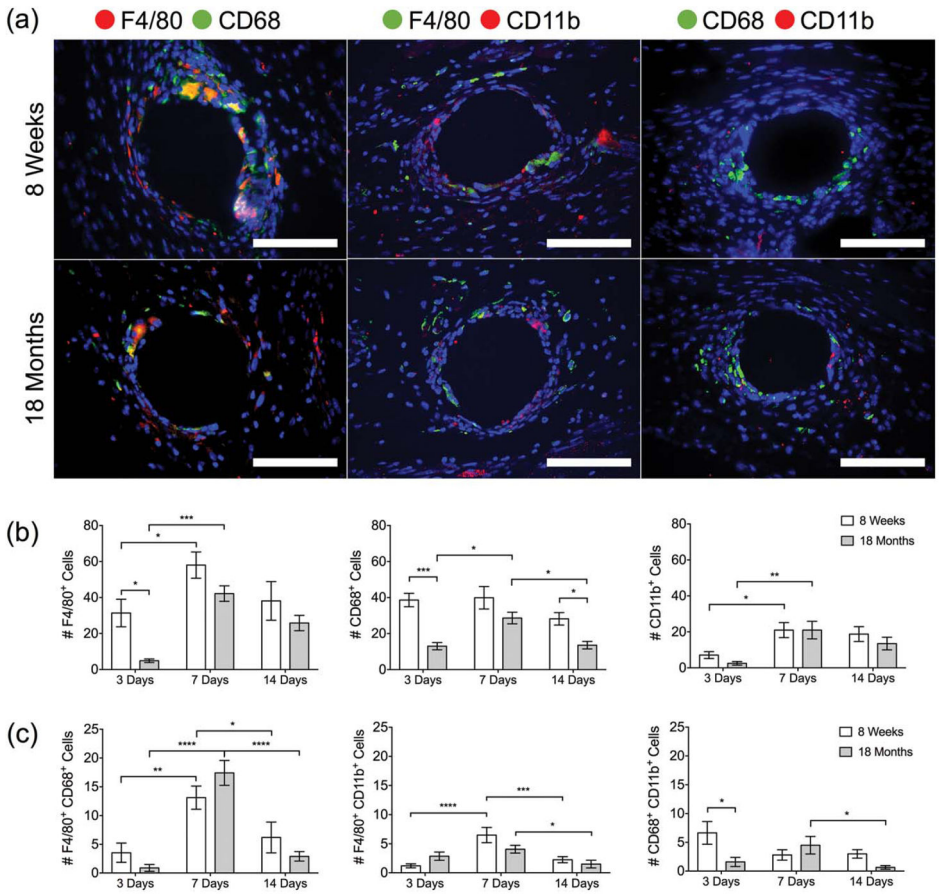

FIGURE 2.

(a) Fluorescence microscopy images of F4/80 CD68, F4/80 CD11b, and CD68 CD11b co-immunolabeled tissue cross-sections at a single mesh fiber at 7 days (additional days can be seen in Supporting Information, Figures 1–3). DAPI was used to stain cell nuclei. Scale bars represent 50 μm. Cell counts of (b) $F4/80^+$, $CD68^+$, and $CD11b^+$ cells and (c) $F4/80^+$ $CD68^+$, $F4/80^+$ $CD11b^+$, and $CD68^+$ $CD11b^+$ cells surrounding single mesh fibers at 3, 7, and 14 days. Bars represent the mean ± SEM. Statistical significance as (*) $p < 0.05$, (**) $p < 0.01$, (***) $p < 0.001$, and (****) $p < 0.0001$. All other differences are nonsignificant. $N = 7$.

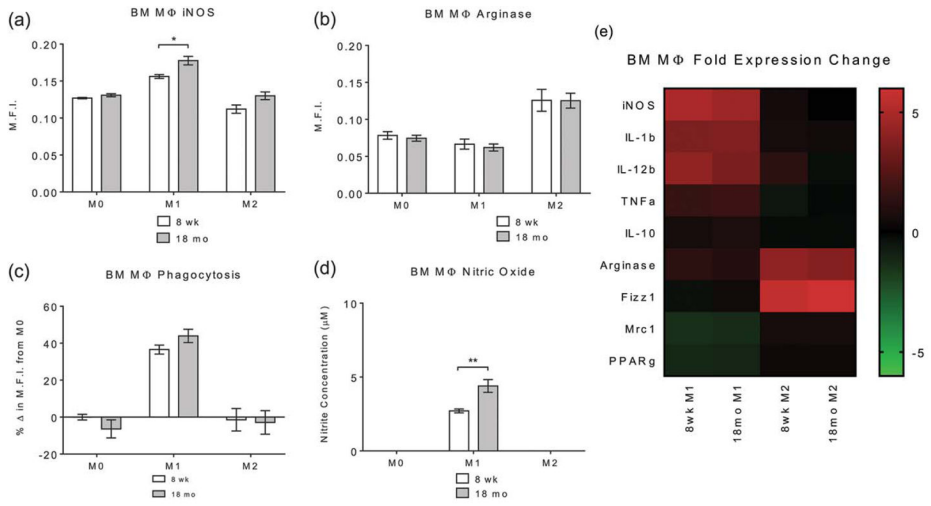

FIGURE 3.

Image analysis of (a) iNOS and (b) Arginase-1 of macrophages treated with media (M0), IFN-γ/LPS (M1), or IL-4 (M2) for 24 h, isolated from 8-week-old and 18-month-old C57BL/6 mice. Representative images are shown in Supporting Information, Figure S5. (c) Phagocytosis function using Vybrant FITC-labeled *E. coli* particles incubated on treated macrophages for 2 h. Representative images are shown in Supporting Information, Figure S5. (d) Nitric oxide production using Greiss reagent system on supernatants from treated macrophages. (e) Taqman gene expression assays assessing the gene expression of pro- and anti-inflammatory gene targets. Bars represent the mean ± SEM. Statistical significance as (*) $p < 0.05$ and (**) $p < 0.01$. All other differences are nonsignificant. $N = 5$.

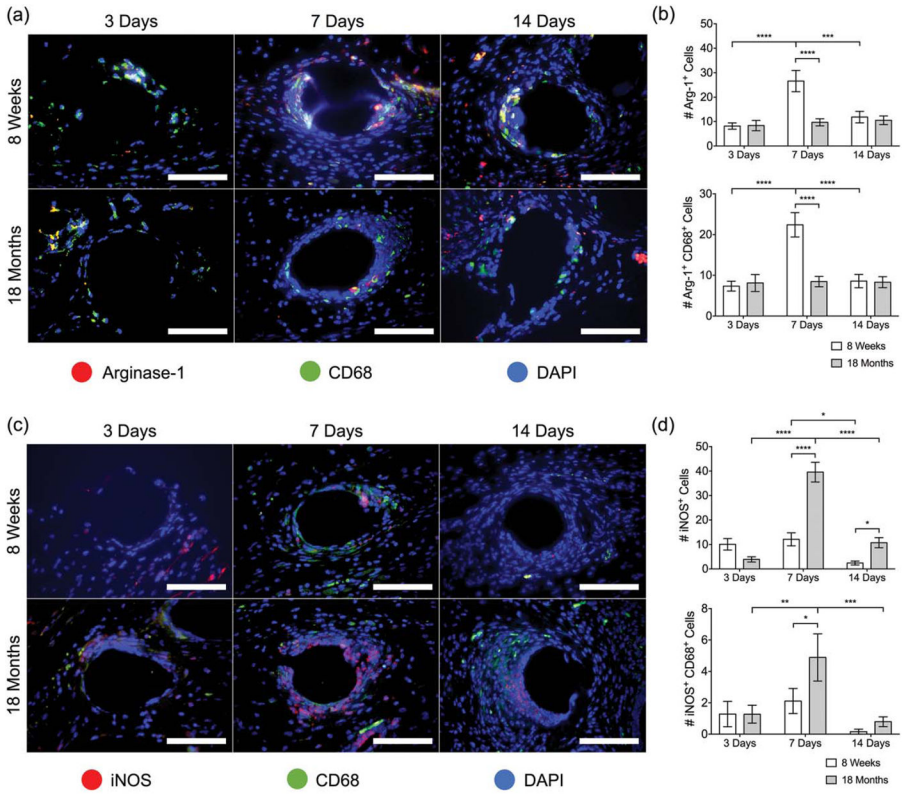

FIGURE 4.

Fluorescence microscopy images of (a) Arginase-1 (red) CD68 (green) co-immunolabeling and (b) iNOS (red) CD68 (green) coimmunolabeling at a single mesh fiber at 3, 7, and 14 days. DAPI was used to stain cell nuclei. Scale bars represent 50 μm. Cell count image analysis of (c) Arg-1$^+$, Arg-1$^+$ CD68$^+$ cells and (d) iNOS$^+$, iNOS$^+$ CD68$^+$ cells at 3, 7, and 14 days. Bars represent the mean ± SEM. Statistical significance as (*) $p < 0.05$, (**) $p < 0.01$, (***) $p < 0.001$, and (****) $p < 0.0001$. All other differences are nonsignificant. $N = 7$.

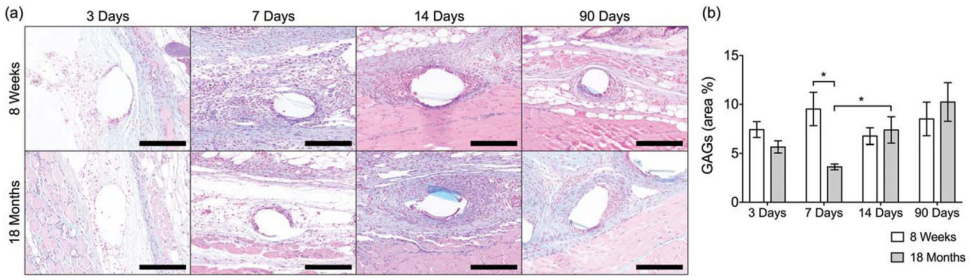

FIGURE 5.

(a) Images of Alcian-Blue-stained tissue cross-sections (GAGs in blue) and (b) image analysis of GAG deposition as percentage of total inflammatory tissue area (excluding skin and muscle) surrounding single mesh fibers at 20× of tissue cross-sections from 8-week-old and 18-month-old mice implanted with a 1 cm^2 piece of polypropylene mesh for 3, 7, 14, and 90 days. Scale bars represent 100 μm. Bars represent the mean ± SEM. Statistical significance as (*) $p < 0.05$. All other differences are nonsignificant. $N = 7$.

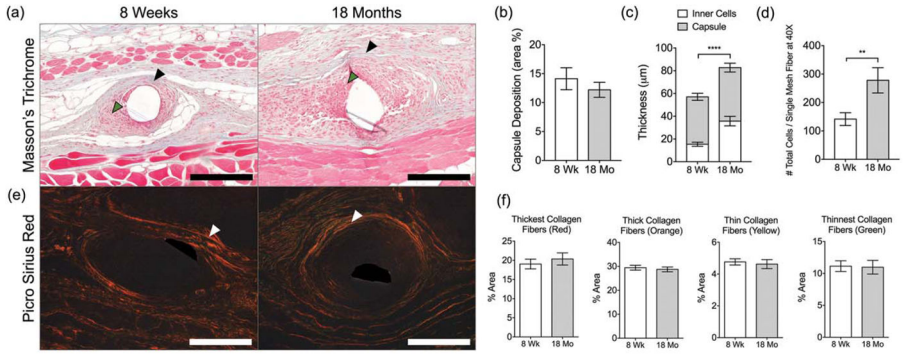

FIGURE 6.

(a) Masson's Trichrome-stained tissue sections of 8-week-old and 18-month-old mice at 90 days. Black and green arrowheads indicate the collagenous portion of the capsule and cellular reaction surrounding single mesh fibers, respectively. Scale bars represent 200 µm. (b) Image analysis of capsule deposition as percentage from the area of inflammatory tissue (excluding skin and muscle). (c) Thickness of capsule, inner cells, and total thickness. (d) Total number of cells surrounding single mesh fibers. (e) Picro Sirius Red-stained tissue sections of 8-week-old and 18-month-old mice at 90 days. White arrowheads indicate the capsule surrounding single mesh fibers. (f) Image analysis of collagen capsule composition surrounding single mesh fibers of samples stained with Picro Sirius Red. Scale bars represent 100 µm. Bars represent the mean ± SEM. Statistical significance as (**) $p < 0.01$ and (****) $p < 0.0001$. All other differences are nonsignificant. $N = 7$.

TABLE I

Primary and Secondary Antibody Combinations and Dilutions Used to Perform Fluorescent Co-Immunolabeling on Tissue Cross-Sections of 8-week and 18-month Mice Implanted with Polypropylene Nesh for 3, 7, and 14 days

Labeling	1°Ab	1°Ab	2°Ab Alexa 594	2°Ab Alexa (488)
$F4/80^+$ $CD68^+$	1:50 (rat F4/80)	1:150 (rabbit CD68)	1:100 (anti-rat)	1:200 (anti-rabbit)
$F4/80^+$ $CD11b^+$	1:50 (rat F4/80)	1:100 (goat CD11b)	1:200 (anti-goat)	1:100 (anti-rat)
$CD11b^+$ $CD68^+$	1:150 (goat CD11b)	1:150 (rabbit CD68)	1:200 (anti-goat)	1:200 (anti-rabbit)
$iNOS^+$ $CD68^+$	1:100 (rabbit iNOS)	1:150 (goat CD68)	1:200 (anti-rabbit)	1:200 (anti-goat)
$Arg\text{-}1^+$ $CD68^+$	1:150 (rabbit Arg-1)	1:150 (goat CD68)	1:400 (anti-goat)	1:200 (anti-goat)

TABLE II

Primary and Secondary Antibody Dilutions Used to Perform Indirect Fluorescent Antibody Labeling of *in vitro* Bone Marrow-Derived Macrophage Cultures

Labeling	1°Ab	2°Ab Alexa (488)
iNOS	1:100 (rabbit iNOS)	1:200 (donkey anti-rabbit)
Arginase	1:200 (rabbit arginase)	1:200 (donkey anti-rabbit)